J. Meas. Sci. Instrum., 2025, 16(2): 280-290.
DOI: 10.62756/jmsi.1674-8042.2025027
http://jmsi.publish.founderss.cn
jmsi@nuc.edu.cn

Estimation method of rotor position of PMSM with filterless high-frequency square-wave injection

JIANG Xiangju*, ZHAI Jilin

School of Automation and Electrical Engineering, Lanzhou Jiaotong University, Lanzhou 730070, China

***Corresponding author:** JIANG Xiangju (jxju16@mail.lzjtu.cn)

Received: November 5, 2023 **Revised:** December 10, 2023 **Accepted:** January 20, 2024

Abstract: For the traditional methods of rotor position estimation for permanent magnet synchronous motor (PMSM), the phase shift caused by the introduction of filter will affect the accuracy of rotor position estimation to some extent. This paper presents an improved rotor position estimation method for high frequency square wave signal injection without filter. Firstly, the traditional method injects high-frequency pulse vibration signals into the estimated shafting, and the proposed method injects high-frequency square wave signals into the estimated shafting to avoid the introduction of filters in the process of extracting rotor position information. Then, the rotor position signal is decoupled in the stationary shafting, and the rotor position error after demodulation is processed by PLL. The system realized the signal processing of rotor position without filter, which improved the convergence speed and estimation precision of rotor position and the dynamic response performance of the system. The simulation results showed that the proposed method had fast convergence speed and small phase delay, and better improved the precision of rotor position detection.

Key words: permanent magnet synchronous motor (PMSM); high-frequency square-wave injection; filter; rotor position; decoupling

0 Introduction

Permanent magnet synchronous motor (PMSM) has the advantages of small size, large starting torque, strong anti-overload ability, and low loss. It has been widely used in high precision control fields such as electric vehicle drive and military application[1]. Three-phase PMSM is a complex nonlinear, strong coupling, and time-varying system. When the motor is greatly affected by its own parameters and external disturbances in the operation process, it often cannot achieve excellent closed-loop control performance. Among them, encoder and other speed sensors need to be installed at the rotating shaft to accurately locate the position of the rotor when the motor is running, and these sensors are mostly mechanical structures, which increases the volume and complexity of the system and is easily damaged[2]. Therefore, the sensorless control technology of PMSM has become a research hotspot in the field of motor control[3-5].

The sensorless control of PMSM is generally divided into two types. One is the mathematical model method based on the fundamental wave mathematical back electromotive force for medium and high speed[6-8], which estimates the position and speed of the rotor by detecting the relevant electrical signals in the stator windings of the motor. The main control algorithms are extended Kalman filter algorithm, model reference adaptive control algorithm, and sliding mode observer algorithm, but these control algorithms can achieve good control performance only when the motor running speed is at medium/high speed[9,10]. When the motor is starting up or running at low-speed, sensorless detection fails due to difficult signal-to-noise ratio extraction.

In order to solve the problem that the motor can also realize the precise positioning of the rotor position under the condition of low speed operation, scholars have turned their research focus to another sensorless detection method using the salient pole effect of the motor[11-13]. The control algorithm is based on the superposition of a high-frequency signal on the fundamental signal of the motor stator winding operation, and realizes the tracking of the rotor position by demodulating the signal. Common high-frequency signal injection methods include rotating high-frequency signal injection into stationary coordinate axes and pulsating high frequency singal injection into estimated synchronous axes[14-19]. They are both high-frequency sinusoidal signal

injection. When the two methods decouple the rotor position signal, the introduction of the band-pass filter and the band-stop filter leads to a delay in the rotor position estimation, which limits the bandwidth of the closed-loop control system and reduces the dynamic performance of the system[20-22].

A rotor position identification method was proposed by injecting a high-frequency square-wave voltage signal into the estimated stator straight axis. By transferring the high frequency square wave voltage signal to the estimated direct axis, the packaging mode of the high frequency response current under the static axis system was found and calculated, so as to determine the position of the rotor. The quadrature phase-locked loop position estimation error was controlled to zero, and the output of the quadrature phase-locked loop was the actual location of the rotor, which realized the observation of the estimated rotor position. The high frequency current and fundamental current were extracted by the filter-free signal separation strategy, which made the error convergence of rotor position estimation faster and significantly improved the dynamic response performance of sensorless control system. The proposed method was verified and analyzed by simulation experiments.

1 Filterless high-frequency square-wave injection principle

Fig.1 is a block diagram of rotor position signal extraction based on filterless high-frequency square-wave signal injection into PMSM. The high-frequency square-wave voltage signal is injected into the estimated stator direct axis, and the rotor position error is decoupled by processing the high-frequency response current signal in the stationary coordinate system, and then the rotor position is estimated by the rotor position observer.

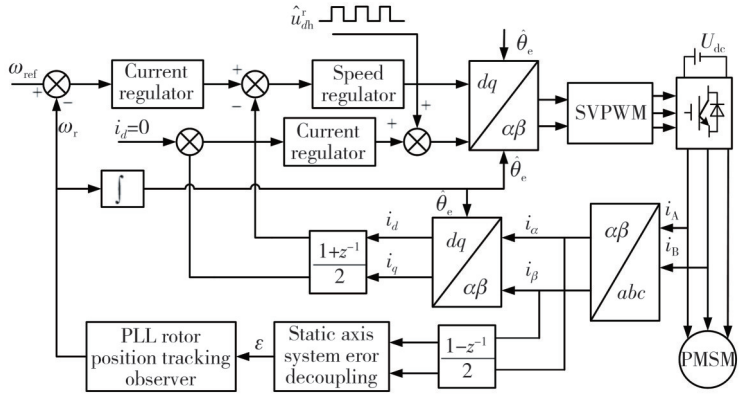

Fig. 1 Block diagram of rotor position signal extraction based on filterless

The stator voltage equation of PMSM under the rotating shaft system is

$$\begin{bmatrix} u_d \\ u_q \end{bmatrix} = \begin{bmatrix} R_s + pL_d & -\omega_f L_q \\ \omega_f L_d & R_s + pL_q \end{bmatrix} \begin{bmatrix} i_d \\ i_q \end{bmatrix} + \begin{bmatrix} 0 \\ \omega_f \psi_f \end{bmatrix}, \quad (1)$$

where u_d, u_q and i_d, i_q are expressed as stator voltage and stator current under synchronous rotation of PMSM shafting; R_s is expressed as stator resistance; L_d, L_q are the direct-axis and quadrature-axis inductances, respectively; ω_f is the electrical angular velocity of the motor rotor; p is represented as a differential operator; ψ_f is expressed as rotor permanent magnet flux linkage.

Since the frequency of the high-frequency signal injected into the stator winding of the motor is generally much higher than the fundamental frequency of the motor during operation, when the motor is in the start-up or low-speed running phase, its motion back EMF is zero. At the same time, ignoring the influence of the stator resistance voltage drop, the mathematical model of PMSM under high-frequency excitation can be equivalent to pure inductive load, that is

$$\begin{bmatrix} u^r_{dh} \\ u^r_{qh} \end{bmatrix} \approx \begin{bmatrix} L_d & 0 \\ 0 & L_q \end{bmatrix} p \begin{bmatrix} i^r_{dh} \\ i^r_{qh} \end{bmatrix}, \quad (2)$$

where u^r_{dh}, u^r_{qh} and i^r_{dh}, i^r_{qh} are expressed as high-frequency voltage and current components under $\hat{d}$-$\hat{q}$ synchronous shafting; h is expressed as a high-frequency quantity; r is denoted as rotor shafting.

A high-frequency signal is injected on the estimated d-axis. In the actual d-q coordinate axis system, it can be expressed as

$$\begin{bmatrix} u^r_{dh} \\ u^r_{qh} \end{bmatrix} = \begin{bmatrix} \cos \theta^*_e & \sin \theta^*_e \\ -\sin \theta^*_e & \cos \theta^*_e \end{bmatrix} \begin{bmatrix} u^{r\wedge}_{dh} \\ u^{r\wedge}_{qh} \end{bmatrix}. \quad (3)$$

The synchronously rotating current term of Eq. (2) can be converted to a stationary shaft system.

$$p \begin{bmatrix} i^r_{dh} \\ i^r_{qh} \end{bmatrix} = T(\theta_e)\, p \begin{bmatrix} i^r_{\alpha h} \\ i^r_{\beta h} \end{bmatrix}. \quad (4)$$

By substituting Eqs. (3) and (4) into Eq. (2), the

high frequency current response of stationary shafting can be expressed as

$$\begin{bmatrix} L_d & 0 \\ 0 & L_q \end{bmatrix} T(\theta_e)\, p \begin{bmatrix} i^r_{\alpha h} \\ i^r_{\beta h} \end{bmatrix} = T(\theta_{err}) \begin{bmatrix} \hat{u}^r_{dh} \\ \hat{u}^r_{qh} \end{bmatrix}. \tag{5}$$

The finishing formula can be obtained by

$$p \begin{bmatrix} i^r_{\alpha h} \\ i^r_{\beta h} \end{bmatrix} = T(\theta_e)^{-1} \begin{bmatrix} \dfrac{1}{L_d} & 0 \\ 0 & \dfrac{1}{L_d} \end{bmatrix} T(\theta_{err}) \begin{bmatrix} \hat{u}^r_{dh} \\ \hat{u}^r_{qh} \end{bmatrix}, \tag{6}$$

where $T(\theta_e)$ is expressed as the transformation matrix from the actual shafting to the stationary shafting; $T(\theta_{err})$ is the transformation matrix from the estimated shafting to the actual shafting.

The estimation error is

$$\theta_{err} = \theta_e - \hat{\theta}_e. \tag{7}$$

The relationship between the actual rotor synchronous shafting d-q of the motor and the estimated rotor synchronous shafting $\hat{d}$-$\hat{q}$ is shown in Fig.2.

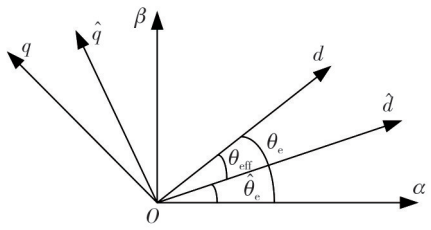

Fig. 2 Relationship between estimated rotor and actual rotor coordinate system

The following high-frequency square-wave voltage signal is injected into the estimated rotor d-axis.

$$\begin{bmatrix} \hat{u}^r_{dh} \\ \hat{u}^r_{qh} \end{bmatrix} = \begin{bmatrix} V_{in}\phi_{spr}(t) \\ 0 \end{bmatrix}, \tag{8}$$

where V_{in} is the amplitude of the injected high-frequency square-wave; $\hat{u}^r_{dh}$ and $\hat{u}^r_{qh}$ are the estimated shaft injected high-frequency voltage component; $\phi_{spr}(t)$ is a unit square-wave piecewise function, and it is

$$\phi_{spr}(t) = \begin{cases} -1, & 0 < \lambda(t) \leqslant \dfrac{T}{2}, \\ 1, & \dfrac{T}{2} < \lambda(t) < T, \end{cases} \tag{9}$$

where T is the period of the injected square-wave signal; $\lambda(t)$ is the remainder of dividing t by T.

Substituting Eq. (7) into Eq. (6), the high-frequency current signal envelope under the stationary coordinate axis system can be obtained by

$$\begin{bmatrix} I_{\alpha enl} \\ I_{\beta enl} \end{bmatrix} = \frac{V_{in}\phi_{spr}(t)}{\omega_h L_d L_q} \begin{bmatrix} L_\tau \cos\hat{\theta}_e - L_\sigma \cos(\theta_e + \theta_{err}) \\ L_\tau \sin\hat{\theta}_e - L_\sigma \sin(\theta_e + \theta_{err}) \end{bmatrix}, \tag{10}$$

where $I_{\alpha enl}$ and $I_{\beta enl}$ are the envelope of the high-frequency response current signal under the stationary shaft system, respectively; ω_h is the frequency of the injected symmetrical high-frequency square-wave voltage signal; L_τ is the mean value of the inductance; L_σ is the difference in inductance.

When the estimated shaft position of the motor rotor coincides with the actual shaft position, at this point, the estimated value of the rotor position converges with the actual value.

$$\begin{bmatrix} I_{\alpha enl} \\ I_{\beta enl} \end{bmatrix} = \frac{V_{in}\phi_{spr}(t)(L_\tau - L_\sigma)}{\omega_h L_d L_q} \begin{bmatrix} \cos\hat{\theta}_e \\ \sin\hat{\theta}_e \end{bmatrix}. \tag{11}$$

It can be seen from Eq. (10) that after extracting the envelope of the high-frequency response current of the stationary shaft system, the position information of the rotor can be obtained directly by calculating the arctangent function.

$$\hat{\theta}_e = \arctan\frac{I_{\alpha enl}}{I_{\beta enl}}. \tag{12}$$

Since the arctangent function is sensitive to the high-frequency response envelope noise when calculating the rotor position angle, it is prone to deviation and poor robustness. Therefore, the estimated rotor position information was processed by a PLL quadrature phase-locked loop under the static shaft system. When the estimated error of the control rotor position was zero, the output of the phase-locked loop was the actual rotor position, which realized the observation and tracking of the rotor position information. Compared with the traditional PID-type Luenberger position tracking observer, the quadrature phase-locked loop position tracking observer had a simpler structure, and avoided the introduction of a low-pass filter when filtering out noise for observation, thereby improving the dynamic response performance of the system. And the estimated rotor position output was not affected by high-frequency harmonics, which ensured the rotor position estimation accuracy.

2 Rotor position estimation strategy for PMSM

2.1 Rotor position error signal decoupling under stationary shafting

The amplitude of the high-frequency response current signal envelope under the static shaft system can be

obtained by

$$\left|I_{\alpha\beta}\right|=\sqrt{I_{\alpha\mathrm{enl}}^2+I_{\beta\mathrm{enl}}^2}=\frac{V_{\mathrm{in}}\phi_{\mathrm{spr}}(t)}{\omega_{\mathrm{h}}L_dL_q}(L_\tau-L_\sigma)=\frac{V_{\mathrm{in}}\phi_{\mathrm{spr}}(t)}{\omega_{\mathrm{h}}L_dL_q}L_q. \tag{13}$$

Through the calculation, it can be known that the estimated error information of the rotor can be expressed as

$$\varepsilon=I_{\beta\mathrm{enl}}\cos\hat{\theta}_{\mathrm{e}}-I_{\alpha\mathrm{enl}}\sin\hat{\theta}_{\mathrm{e}}=\frac{V_{\mathrm{in}}\phi_{\mathrm{spr}}(t)}{\omega_{\mathrm{h}}L_dL_q}L_\sigma\sin\left(\theta_{\mathrm{e}}+\theta_{\mathrm{err}}+\hat{\theta}_{\mathrm{e}}\right)=\frac{V_{\mathrm{in}}\phi_{\mathrm{spr}}(t)}{\omega_{\mathrm{h}}L_dL_q}L_\sigma\sin(2\theta_{\mathrm{err}}). \tag{14}$$

In order to improve the accuracy of rotor position error and reduce the influence of dead-time effect of inverter, it is usually treated by normalization. Thus, the estimation error can be expressed as

$$\varepsilon=\frac{I_{\beta\mathrm{enl}}\cos\hat{\theta}_{\mathrm{e}}-I_{\alpha\mathrm{enl}}\sin\hat{\theta}_{\mathrm{e}}}{\left|I_{\alpha\beta}\right|}=\frac{\left(L_d-L_q\right)}{2L_{\mathrm{q}}}\sin(2\theta_{\mathrm{err}}). \tag{15}$$

When the estimated value of the rotor position converges to the actual value, the error is zero, then the estimated error including only the rotor is

$$\varepsilon=\frac{L_q-L_d}{L_q}\theta_{\mathrm{err}}. \tag{16}$$

The processing flow of rotor position information on stationary shafting is shown in Fig.3.

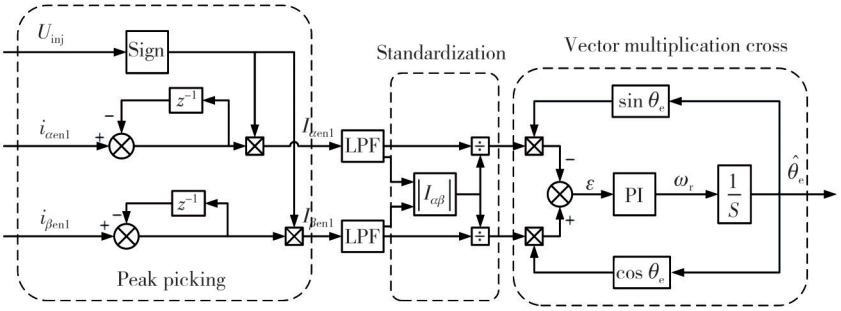

Fig. 3 Static shaft system error signal decoupling box diagram

2.2 Filterless rotor position signal separation strategy

Usually, the high-frequency response current vector needs to be separated from the signal carrier. When extracting the fundamental current required by the current controller and extracting the high-frequency current component, a low-pass filter and a band-pass filter are used, respectively, resulting in the system being filtered. The rotor error estimation accuracy decreases due to the phase lag of the rotor, which reduces the dynamic performance of the system in the process of rotor position detection.

A filterless signal separation strategy was proposed, and the frequency of the injected square-wave signal was selected to be consistent with the switching frequency of the inverter. At two adjacent sampling moments, the amplitudes of the high-frequency current responses were equal and opposite in sign. At the same time, the frequency of the high-frequency square-wave injected by the estimated shaft was much higher than the fundamental wave frequency when the motor was running. Therefore, the magnitude of the fundamental wave current signal at two adjacent sampling moments was a constant value. Fig.4 is the vector sequence diagram of carrier PWM, injected high-frequency square-wave voltage signal, and high-frequency response current signal.

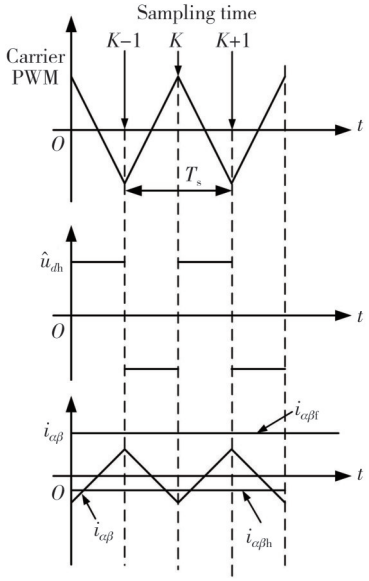

Fig. 4 Timing diagram of high-frequency voltage signal and response current signal

Therefore, under the stationary shaft system, the fundamental current, the high-frequency current component, and the high-frequency current vector between two adjacent sampling moments satisfy

$$\begin{cases}\boldsymbol{i}_{\alpha\beta}(k-1)=\boldsymbol{i}_{\alpha\beta\mathrm{f}}+\boldsymbol{i}_{\alpha\beta\mathrm{h}},\\ \boldsymbol{i}_{\alpha\beta}(k)=\boldsymbol{i}_{\alpha\beta\mathrm{f}}-\boldsymbol{i}_{\alpha\beta\mathrm{h}},\end{cases} \tag{17}$$

where $\boldsymbol{i}_{\alpha\beta\mathrm{f}}$, $\boldsymbol{i}_{\alpha\beta}$, and $\boldsymbol{i}_{\alpha\beta\mathrm{h}}$ are expressed as high-frequency current vector, fundamental current, and high-frequency current components, respectively.

Using the filterless carrier signal separation strategy, the fundamental feedback current and the high-frequency response current are obtained through simple algebraic operations.

$$\boldsymbol{i}_{\alpha\beta\mathrm{h}}(k)=\frac{\boldsymbol{i}_{\alpha\beta}(k-1)-\boldsymbol{i}_{\alpha\beta}(k)}{2}, \tag{18}$$

$$\boldsymbol{i}_{\alpha\beta\mathrm{f}}(k)=\frac{\boldsymbol{i}_{\alpha\beta}(k-1)+\boldsymbol{i}_{\alpha\beta}(k)}{2}. \tag{19}$$

We can know that the fundamental current and high-frequency current components in the synchronous coordinate system can be obtained by simple mathematical calculation of the adjacent current sampling, without band-pass and band-stop filter for carrier separation of the signal, so as to improve the bandwidth of the system and the convergence speed and accuracy of the rotor position tracking observer.

3 Magnetic pole polarity identification

The initial value of the rotor position can be obtained. However, since the estimated value of the rotor position is a multi-solution value with a period of p, the position of the magnetic pole axis may be the real rotor position. It may also differ by 180° mechanical angle. If the initial position estimation of the rotor is inaccurate, the starting torque of the motor will be small, causing the motor to lose steps or even reverse. Therefore, it is necessary to determine the magnetic pole polarity for the rotor position. At present, there are mainly positive and negative pulse voltage injection method[23] and applied current bias method[24] for rotor magnetic pole polarity discrimination. Its application principle is based on the nonlinear saturation magnetization characteristics of the stator core. Fig.5 is the schematic diagram of judging the polarity of rotor magnetic poles based on the saturation characteristics of the stator core.

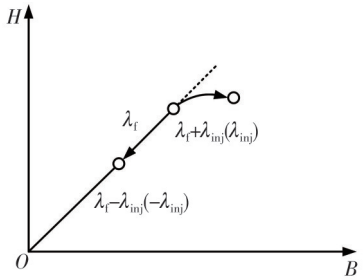

Fig. 5 Schematic diagram of judging rotor magnetic poles polarity based on nonlinear saturation characteristics of stator core

The positive and negative pulse voltage method is used to identify the polarity. Based on the initial value of the rotor magnetic pole position obtained by the high-frequency square-wave injection method, the pulse voltage vectors with opposite directions and equal magnitudes are injected into the stator windings of the motor, respectively. When the magnetic field generated by the permanent magnet is in the same direction as the magnetic field generated by the stator winding current, the strength of the air gap magnetic field increases, the saturation degree of the stator core increases, and the magnetic permeability decreases. The slope of any point of the saturation characteristic curve represents the d-axis stator inductance, so that the stator inductance is reduced. The judgment of the magnetic pole polarity of the rotor is achieved by detecting the length of time that the response current of the two excitations decays to zero.

When the motor is stationary, the d-axis circuit can be equivalent to a first-order R-L series circuit, as shown in Fig.6.

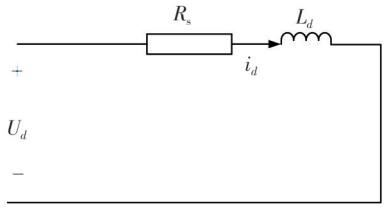

Fig. 6 First-order R-L series circuit

The time constant of the straight-axis equivalent circuit is

$$\tau=\frac{L_d}{R_\mathrm{s}}. \tag{20}$$

When the injection direction of the pulse voltage is $\hat{\theta}_\mathrm{e}$, the magnetic circuit is saturated. According to the inductor saturation effect, it can be known that $L_d=L_d^+$. The time constant of the circuit is τ_N. If the injection direction is $\hat{\theta}+\pi$, the magnetic circuit of the stator core will not be saturated. At this time $L_d=L_d^-$, the time constant of the circuit is τ_S. Due to $L_d^+<L_d^-$, the time for the response current to decay from the steady state value to zero for the two pulse excitations is t^+ and t^-, the injection direction with a shorter time is the actual motor direct axis direction. Then the angle compensation is performed according to the initial judgment value of the rotor magnetic pole axis. If $t^+<t^-$, then the estimated direct axis direction is the actual direct axis direction. At this time $\hat{\theta}=\hat{\theta}_\mathrm{e}$, no angle compensation is required. As shown in Fig.7 (a), if $t^+>t^-$, then the estimated direct axis direction is opposite to the actual direct axis direction. At this time $\hat{\theta}=\hat{\theta}_\mathrm{e}+\pi$, the compensation angle is π, as shown in Fig.7 (b).

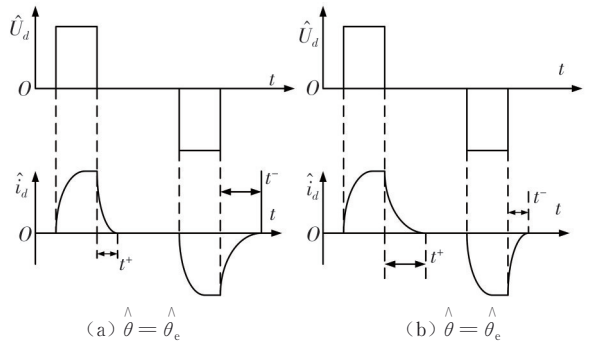

Fig. 7 Schematic diagram of positive direction judgment of actual straight axis

Based on the initial judgment value $\hat{\theta}_e$ of the rotor position obtained by the high-frequency square-wave voltage signal injection method, a voltage pulse vector of equal magnitude and reverse is injected into the stator winding of the motor. Fig. 8 is the implementation process of judging the polarity of the magnetic pole by the voltage pulse vector injection method. The flow chart of the whole system processing is shown in Fig.9.

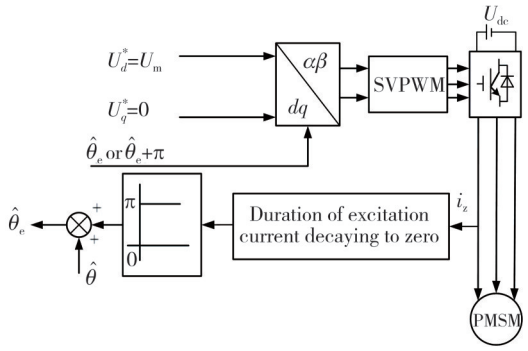

Fig. 8 Schematic diagram of rotor pole polarity identification

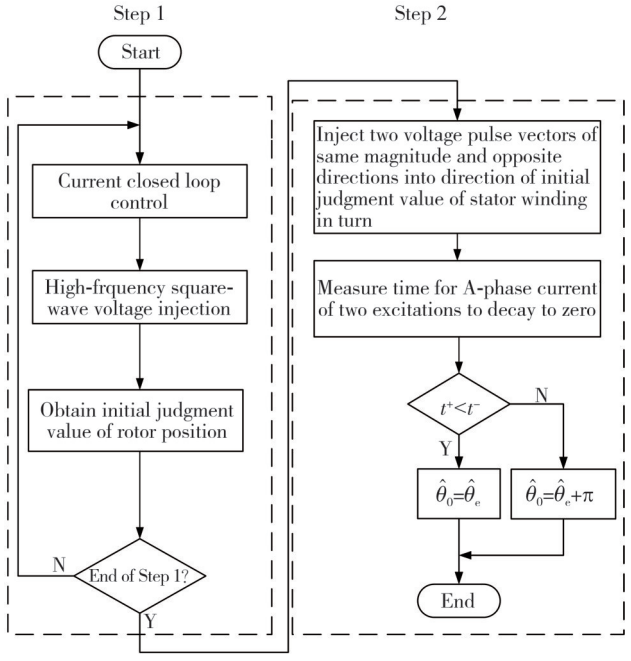

Fig. 9 Rotor position estimation process flowchart

4 Simulation results

As an energy-saving and environmentally friendly vehicle, electric vehicle has been favored by industry in recent years. As the core of electric vehicles, motor drive system has a profound impact on the performance of the vehicle. This experiment used simulation analysis[25].

In order to verify the accuracy of the high-frequency square-wave injection strategy without filter signal separation proposed in this paper, the sensorless control system of PMSM with pulsating high-frequency signal injection and high-frequency square-wave injection under zero/low speed operation was simulated and compared. The simulation model of PMSM was built in Matlab/simulink environment. Fig. 10 is simulation model of pulsating high-frequency singal injection method. Fig.11 is the simulation model of the rotor position observer when the pulsating high-frequency signal is injected. Fig. 12 is simulation model of filterless high-frequency square-wave signal injection method. Fig. 13 is the rotor position decoupling simulation model when high-frequency square-wave is injected. The parameters used in the motor simulation are shown in Table 1.

Table 1 PMSM parameters for simulation

Parameter	Numerical value
Rated power/kW	15
Rated voltage/V	380
Rotor flux/Wb	0.094 1
Damping coefficient/(N•m•s)	0.008
Moment of inertia/(kg•m^2)	0.008
Number of pole pairs	3
Direct axis inductance/mH	0.3
Quadrature inductance/mH	0.8
Stator resistance/Ω	0.551
Rated speed/(r•min^{-1})	3 000

Set the motor load torque to 1 N·m (30% rated torque). The inverter switching frequency is 20 kHz, and the amplitudes of the injected pulsating high-frequency signal and high-frequency square-wave signal are both 25 V. The frequency of the injected pulsating high-frequency signal is 1 000 Hz and the frequency of the injected high-frequency square-wave signal is 10 kHz. Set the parameter values of the PI controller in Fig.3, $k_p=0.012$, $k_i=0.073\,7$.

Fig. 14 show the simulation comparison of the actual position and estimated position of the rotor. Fig. 14(a) shows that the estimated position of the rotor lags 4.2° mechanical angle of the actual position of the rotor when the high-frequency square-wave injection is improved. Fig.14(b) shows that the maximum estimated position of the rotor lags 5.4° mechanical angle of the actual position.

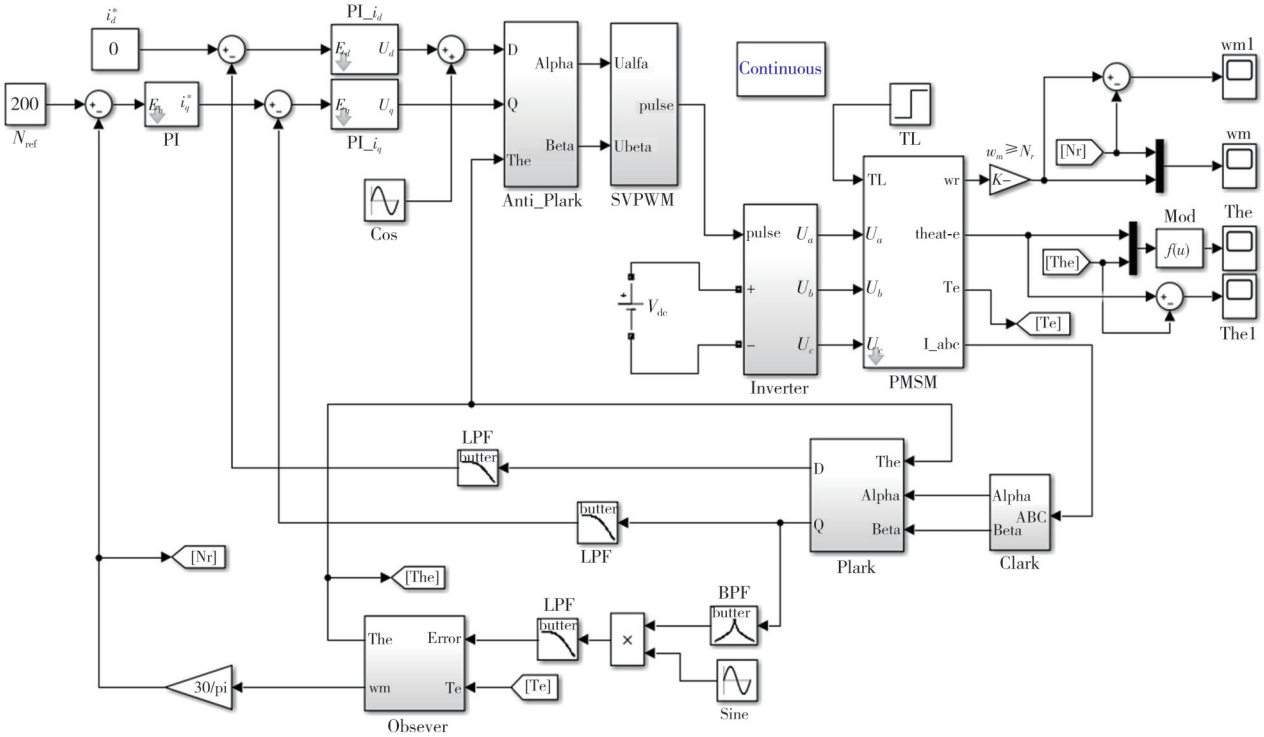

Fig. 10 Simulation model of pulsating high-frequency signal injection method

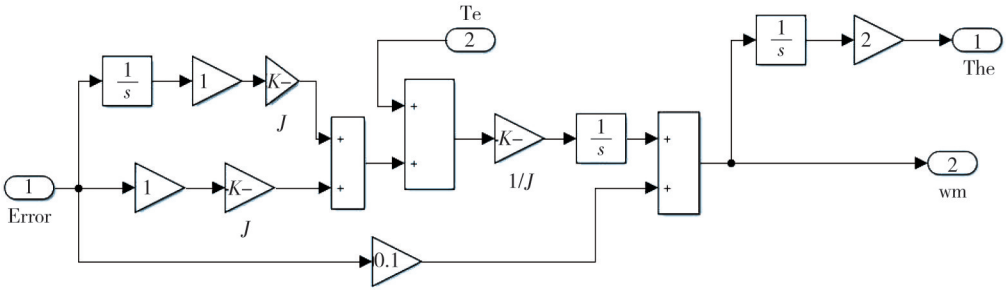

Fig. 11 simulation model of rotor position observer when pulsating high-frequency signal is injected

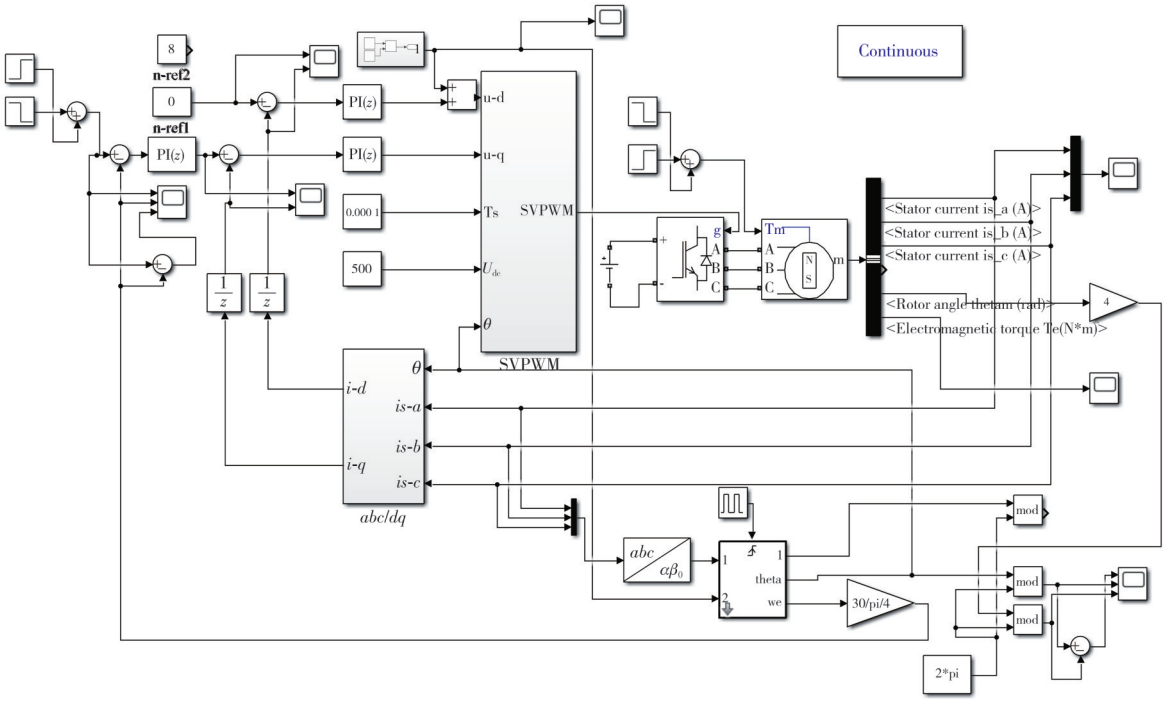

Fig. 12 Simulation model of filterless high-frequency square-wave signal injection method

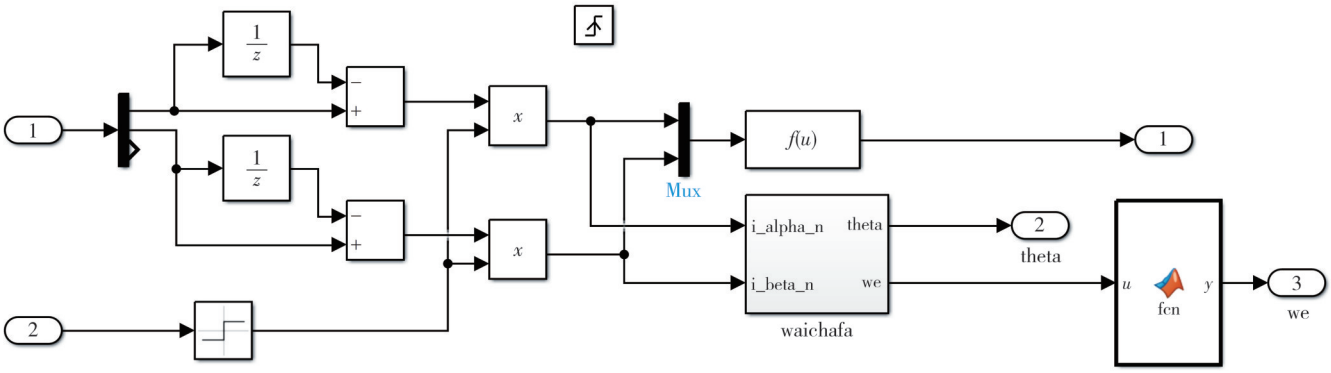

Fig. 13 Rotor position decoupling simulation model when high-frequency square-wave is injected injection method

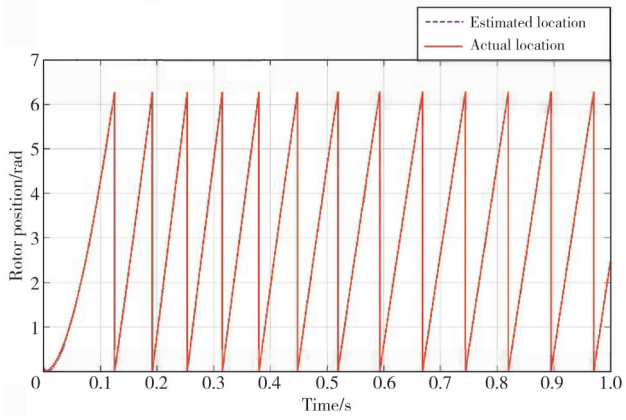

(a) Actual and estimated rotor position at 200 r/min

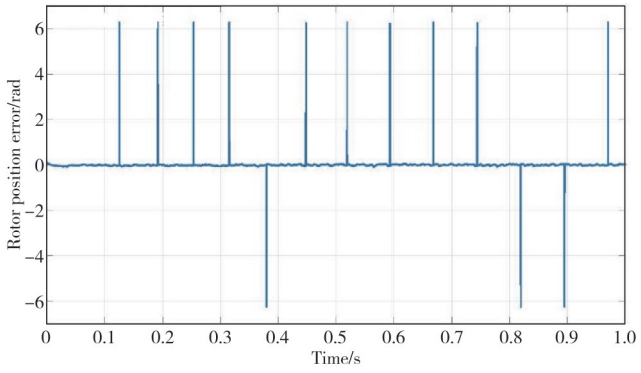

(b) Error between actual rotor position and estimated position at 200 r/min

Fig. 14 Simulation results of high-frequency square-wave signal injection method at 200 r/min

Fig. 15 shows the simulation comparison of the rotor position error by using the filterless high-frequency square-wave signal injection method and the pulsating high-frequency signal injection method when the motor speed is set to 200 r/min. When the pulsating high-frequency singal injection is used, it can be seen from Fig. 15(a) that the estimated position of the rotor obviously lags behind the actual position of the rotor at 13.4° mechanical angle. From Fig. 15(b), it can be seen that the average value of the position estimation error is 11.5° mechanical angle.

Figs. 16 and 17 show the actual position and estimated position of the rotor obtained by the pulsating high-frequency signal injection method and the high-frequency square-wave signal injection method proposed in this paper when the reference speed of the simulated motor changes abruptly under actual operating conditions.

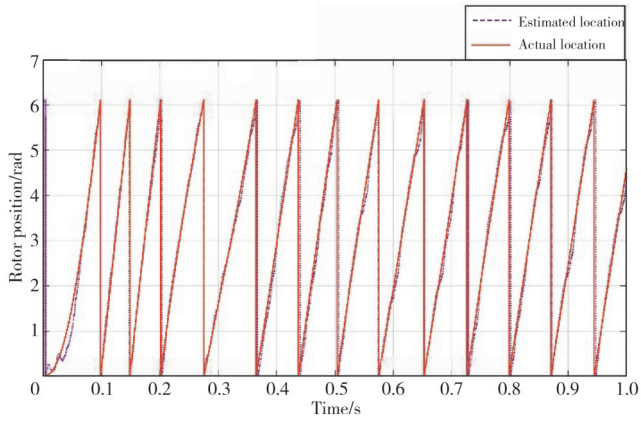

(a) Actual and estimated rotor position at 200 r/min

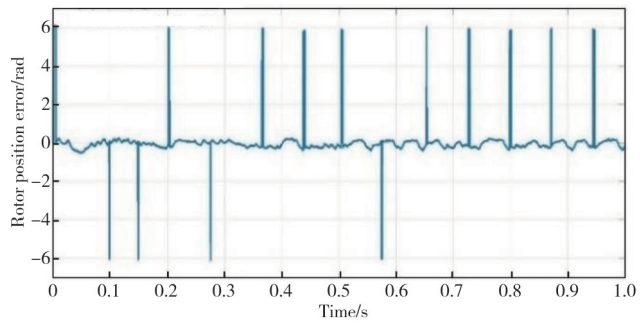

(b) Error between actual rotor position and estimated position at 200 r/min

Fig. 15 Simulation results of pulsating high-frequency signal injection method at 200 r/min

As can be seen from Fig. 16, when injecting pulsating high-frequency signals, the given initial reference speed is 150 r/min. The motor starts from zero speed and reaches a stable state at about 0.62 s. The speed error is ±19 r/min. The rotor angle error is 16° within 0.38 s. The steady state is reached when the reference speed is suddenly increased to 350 r/min. The speed error was ±20 r/min, and the angle error was between −7° and 10° mechanical angle. It can be seen from Fig. 17 that when the high-frequency square-wave signal is injected, the initial given reference speed is 150 r/min. The motor starts from zero speed and

reaches a stable state at about 0.13 s. The speed error is about ±5 r/min, and the rotor angle error is ±3.4° mechanical angle. After 1 s, the reference speed suddenly increases to 350 r/min, the rotor angle error is controlled within ±2° mechanical angle.

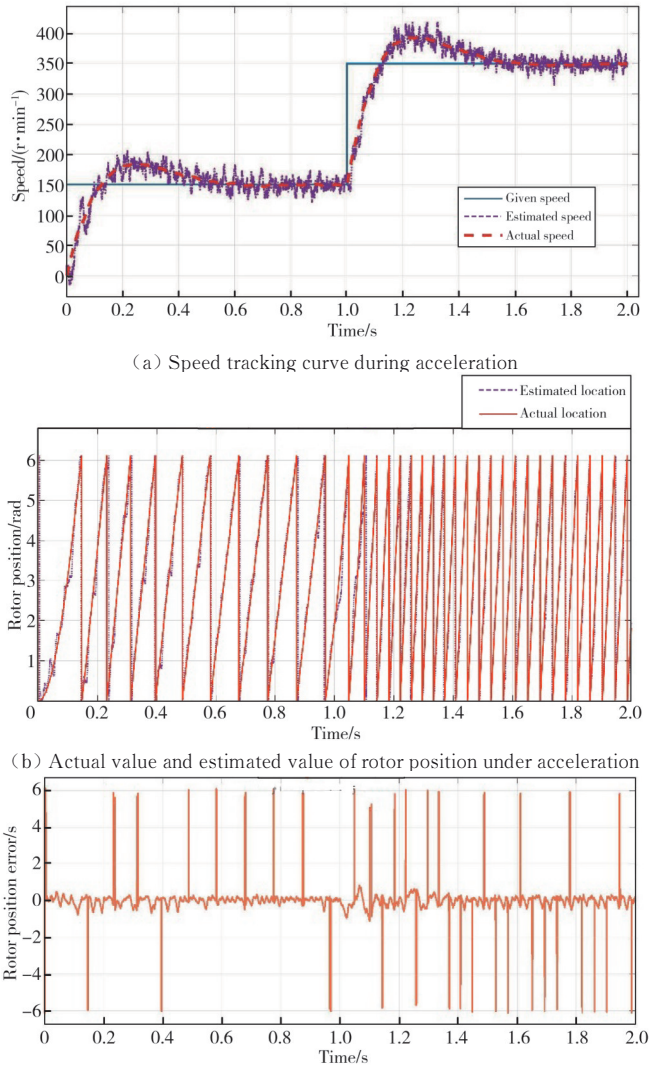

(a) Speed tracking curve during acceleration

(b) Actual value and estimated value of rotor position under acceleration

(c) Rotor position tracking and error under acceleration

Fig. 16 Simulation results of pulsating high-frequency signal injection method under acceleration

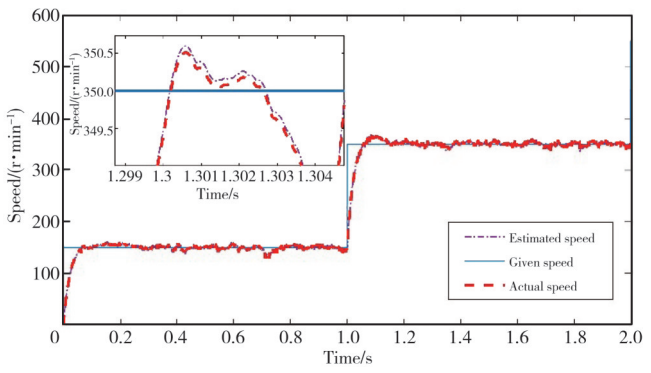

(a) Speed tracking curve during acceleration

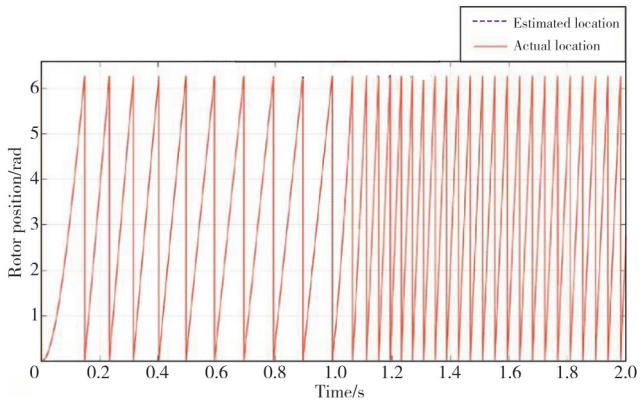

(b) Actual value and estimated value of rotor position at acceleration

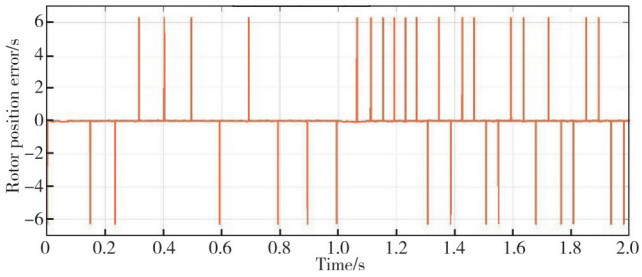

(c) Rotor position tracking and error at acceleration

Fig. 17 Simulation results of high-frequency square-wave injection method under acceleration

It can be seen that the proposed method has better steady-state tracking performance and faster response speed than the pulsating high-frequency signal injection method, and the rotor phase error is smaller and the accuracy is higher. It can better meet the needs of rotor position detection.

5 Conclusions

A rotor position estimation method was proposed based on the injection of a filterless high-frequency square-wave signal. The proposed method used the non-filter signal separation strategy in the decoupling process of the rotor position error signal, and effectively overcame the problem that the traditional pulsed high-frequency signal injection method reduced the identification accuracy of the rotor estimated position due to the phase shift of the low-pass filter and the bandpass filter. The simulation results showed that the proposed method had good steady-state tracking performance, and improved the convergence speed and accuracy of the rotor position observer so that it had a smaller phase error.

Acknowledgement

This work was supported by National Natural Science Foundation of China (No. 61863023); Lanzhou Talent Innovation and Entrepreneurship Project Task Contract

(No. 2019-RC-103).

Declaration of conflicting interests

The authors have no conflict of interests related to this publication.

References

[1] KWON Y C, SUL S K, BALOCH N A, et al. Improved design of IPMSM for sensorless drive with absolute rotor position estimation capability. IEEE Transactions on Industry Applications, 2016, 52(2): 1441-1451.

[2] BOLOGNANI S, CALLIGARO S, PETRELLA R, et al. Sensorless control of IPM motors in the low-speed range and at standstill by HF injection and DFT processing. IEEE Transactions on Industry Applications, 2011, 47(1): 96-104.

[3] LIU J L, XIAO F, SHEN Y, et al. Position-sensorless control technology of permanent-magnet synchronous motor-a review. Transactions of China Electrotechnical Society, 2017, 32(16): 76-88.

[4] BATZEL T D, LEE K Y. Slotless permanent magnet synchronous motor operation without a high resolution rotor angle sensor. IEEE Transactions on Energy Conversion, 2000, 15(4): 366-371.

[5] XU P L, ZHU Z Q. Carrier signal injection-based sensorless control for permanent magnet synchronous machine drives with tolerance of signal processing delays. IET Electric Power Applications, 2017, 11(6): 1140-1149.

[6] ZHANG G Q, WANG G L, NI R G, et al. Adaptive linear element filtering based rotor position observer for interior permanent magnet synchronous motors. Transactions of China Electrotechnical Society, 2016, 31(6): 47-54.

[7] WANG K, CHEN B, SHEN G T, et al. Online updating of rotor time constant based on combined voltage and current mode flux observer for speed-sensorless AC drives. IEEE Transactions on Industrial Electronics, 2014, 61(9): 4583-4593.

[8] WANG G L, YANG R F, YU Y, et al. Position sensorless control for interior permanent magnet synchronous motor. Proceedings of the CSEE, 2010, 30(30): 93-98.

[9] WANG X C, XIE W, KENNEL R, et al. Sensorless control of a novel IPMSM based on high-frequency injection//2013 15th European Conference on Power Electronics and Applications, September 2-6, 2013, Lille, France. New York: IEEE, 2013: 1-8.

[10] GENDUSO F, MICELI R, RANDO C, et al. Back EMF sensorless-control algorithm for high-dynamic performance PMSM. IEEE Transactions on Industrial Electronics, 2010, 57(6): 2092-2100.

[11] YOON Y D, SUL S K, MORIMOTO S, et al. High-bandwidth sensorless algorithm for AC machines based on square-wave-type voltage injection. IEEE Transactions on Industry Applications, 2011, 47(3): 1361-1370.

[12] GAO H W, YU Y J, CHAI F, et al. Position sensorless control of interior permanent magnet synchronous motor based on carrier frequency component method. Proceedings of the CSEE, 2010, 30(18): 91-96.

[13] YAO P Y, FENG G D, WU X, et al. High precision initial rotor position estimation method for permanent magnet synchronous motor based on nonlinear modeling and fitting. Electric Machines and Control, 2024, 28(2): 142-151.

[14] LI H Y, ZHANG X, YANG S Y, et al. A detecting algorithm for initial position of interior permanent magnet synchronous motor based on rotating high frequency injection. Transactions of China Electrotechnical Society, 2018, 33(8): 1723-1731.

[15] WANG X C, XIE W, DAJAKU G, et al. Position self-sensing evaluation of novel CW-IPMSMs with an HF injection method. IEEE Transactions on Industry Applications, 2014, 50(5): 3325-3334.

[16] RACA D, GARCIA P, REIGOSA D D, et al. Carrier-signal selection for sensorless control of PM synchronous machines at zero and very low speeds. IEEE Transactions on Industry Applications, 2010, 46(1): 167-178.

[17] CHOI J, NAM K, BOBTSOV A A, et al. Robust adaptive sensorless control for permanent-magnet synchronous motors. IEEE Transactions on Power Electronics, 2016, 32(5): 3989-3997.

[18] ZHU J, TIAN M, FU R B, et al. Research on rotor position of permanent magnet synchronous motor based on carrier frequency component. Power System Protection and Control, 2015, 43(14): 48-54.

[19] LUO X, TANG Q, SHEN A, et al. Permanent magnet synchronous motor sensorless control by injecting hf pulsating carrier signal into estimated fixed-frequency rotating reference frame. IEEE Transactions on Industrial Electronics, 2016, 63(4): 2294-2303.

[20] WAN S M, WU F, HUANG S H. Initial rotor position estimation of permanent magnet synchronous motor based on high frequency voltage signal injection method. Proceedings of the CSEE, 2008, 28(33): 82-86.

[21] GUO L, YANG Z P, LIN F. A sensorless control strategy for high frequency signal injection permanent magnet synchronous motor with error compensation. Transactions of China Electrotechnical Society, 2019, 34(21): 4458-4466.

[22] YANG J, YANG S Y, LI H Y, et al. Initial rotor position estimation for IPMSM based on high frequency rotating voltage injection. Transactions of China Electrotechnical Society, 2018, 33(15): 3547-3555.

[23] LIU J L, LU J D. High-precision estimation method of initial rotor position for IPMSM based on phase difference of positive and negative sequence current component. Transactions of China Electrotechnical Society, 2016, 31(23): 63-69.

[24] CHEN L, GÖTTING G, DIETRICH S, et al. Self-sensing control of permanent-magnet synchronous machines with multiple saliencies using pulse-voltage-injection. IEEE

Transactions on Industry Applications, 2016, 52(4): 3480-3491.

[25] WANG C Y, XIA J K, SUN Y B. Modern motor control technology. Beijing: Machinery Industry Press, 2014.

无滤波器高频方波注入永磁同步电机转子位置的估计方法

姜香菊*, 翟继林

兰州交通大学 自动化与电气工程学院, 甘肃 兰州 730070

摘　要： 传统的脉振高频信号注入永磁同步电机(PMSM)转子位置估计方法中，引入滤波器产生的相移会对转子位置估计精度产生一定的影响。本文提出了一种改进的无滤波器高频方波信号注入的转子位置估计方法。首先，传统方法在估计的轴系注入脉振高频信号，本文所提方法在估计的轴系中注入高频方波信号，在转子位置信息提取环节中避免了滤波器的引入。然后，在静止的轴系对转子位置信号进行解耦，对解调后的转子位置误差采用PLL锁相环处理。系统实现了无滤波器转子位置信号处理，提升了转子位置的收敛速度和估计精度以及系统的动态响应性能。仿真实验结果表明，所提的方法收敛速度快，相位延迟小，较好的提升了转子位置检测精度。

关键词： 永磁同步电机；高频方波注入；滤波器；转子位置；解耦

引用格式： JIANG Xiangju, ZHAI Jilin. Estimation method of rotor position of PMSM with filterless high-frequency square-wave injection. Journal of Measurement Science and Instrumentation, 2025, 16(2): 280-290. DOI: 10.62756/jmsi. 1674-8042.2025027